



# Electrocrystallisation of zinc from acidic sulphate baths; A nucleation and crystal growth process

D. Vasilakopoulos<sup>\*,1</sup>, M. Bouroushian<sup>1</sup>, N. Spyrellis<sup>1,2</sup>

Laboratory of General Chemistry, School of Chemical Engineering, National Technical University of Athens, 9 Heron Polytechniou, Zografos Campus, GR-15780 Athens, Greece

## ARTICLE INFO

### Article history:

Received 21 December 2007

Received in revised form 7 September 2008

Accepted 26 November 2008

Available online 3 December 2008

### Keywords:

Electrocrystallisation

Nucleation

Crystal growth

Zinc electrodeposition

Chronoamperometry

## ABSTRACT

The electrochemical nucleation and growth of zinc on low-carbon steel from acidic (pH 2.0–4.5) baths containing ZnSO<sub>4</sub>, NaCl, and H<sub>3</sub>BO<sub>3</sub>, was studied by means of chronoamperometry at various cathodic potentials under a charge-transfer controlled regime. It is shown that at overpotentials in the range 0.30–0.55 V (negative to the Zn<sup>2+</sup>/Zn redox value) the electrodeposition proceeds by instantaneous three-dimensional nucleation, which turns to progressive at higher overpotentials and/or very acidic baths. At low cathodic overpotentials (<0.30 V), a two-dimensional contribution limited by the incorporation of Zn ad-atoms in the developing lattice becomes significant at the early stages of deposition, and is more progressive in type the more acidic is the bath pH. Nucleation rate constants were calculated and correlated analytically with the respective potentials, using the classical theory of heterogeneous nucleation, which though fails to lead to reasonable values for the critical nucleus size.

© 2008 Elsevier Ltd. All rights reserved.

## 1. Introduction

During electrochemical metal deposition the microstructure of the new metal phase is determined by the nature of nucleation and growth, and hence various properties of the deposit, i.e. those related to adhesion, behaviour under mechanical stresses or resistance to corrosion, may be amended by a finely tuned deposition process. One of the most important factors in this connection is the substrate effect as severely affects the initial stages of deposition.

Zinc deposits on metals, especially on steel, are widely used to improve corrosion resistance, formability and paintability. The electrodeposition of zinc from acidic sulphate baths has been practiced for long time. Although the dependence of texture and morphology of as-obtained coatings on electrochemical parameters have been investigated in several works [1–7], those that attempt to get an insight into the nucleation and crystal growth process are very few [4,8–10]. Raeissi et al. [4], in their study of the electrochemical nucleation of zinc on steel in sulphate solutions of different pH values, attributed the changes in the crystallographic texture of the deposits to the alteration of the nucleation mode due to hydroxide adsorption. It was shown that at pH 2 instantaneous nucleation was predominant, while at pH 4 it was close to pro-

gressive. Alvarez et al. [8] interpreted the nucleation and growth of zinc on highly oriented pyrolytic graphite in sulphate solutions considering instantaneous nucleation on active sites and diffusion-controlled three-dimensional (3D) growth. Torrent-Burgués et al. [9] performed zinc electrodeposition from sulphate-tartrate baths on vitreous carbon electrode. Their analysis of the current–time transients combined with SEM characterisation indicated instantaneous nucleation with two-dimensional (2D) growth at the initial stages, with a nucleus density in the order of 10<sup>9</sup> cm<sup>-2</sup>. Gomes et al. [10] studied zinc electrodeposition on steel using chronoamperometric and AFM techniques. Near the equilibrium redox potential, zinc underpotential deposition was found to follow the Stranski-Krastanov growth, while the formation of different-sized circular aggregates of random distribution implied that the nucleation was progressive. In the domain of overpotential deposition of zinc, a 3D growth controlled by diffusion along with instantaneous nucleation was seen to prevail.

In the present work, the electrocrystallisation of zinc on low-carbon steel from an acidic sulphate solution is investigated by means of chronoamperometric curves. Furthermore, it is attempted to connect the specific nucleation and growth mechanism with the development of certain crystallographic textures.

## 2. Experimental

Electrochemical measurements were carried out in a single compartment, open air, thermostat-controlled three-electrode cell connected to a WENKING PGS95 galvanopotentioscan system, interfaced with a PC for data acquisition. Low-carbon stainless

\* Corresponding author. Tel.: +30 2107724048; fax: +30 2107723088.

E-mail address: [dimvass@central.ntua.gr](mailto:dimvass@central.ntua.gr) (D. Vasilakopoulos).

<sup>1</sup> ISE member.

<sup>2</sup> Deceased on November 16th 2008, while this paper was under review. The authors would like to dedicate this work to his memory.

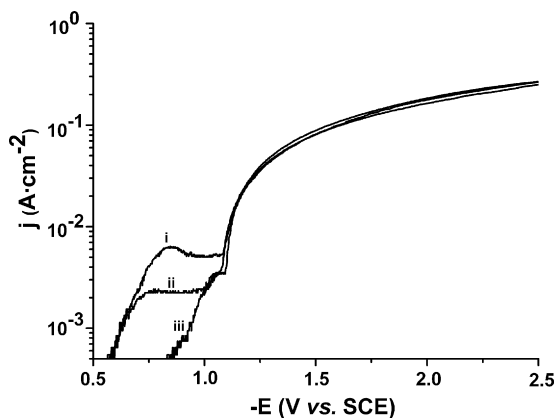


**Fig. 1.** Polarisation curves (scan rate:  $0.01 \text{ V s}^{-1}$ ) with a stationary low-carbon steel electrode in the typical sulphate deposition bath at  $50^\circ\text{C}$ ; pH 2.0 (i), pH 2.5 (ii), and pH 4.0 (iii).

steel (SS316L) cylinders with  $1.54 \text{ cm}^2$  area were used as working electrodes, a Pt grid as counter electrode and a saturated calomel electrode (SCE) as reference. All potentials are reported with respect to this reference. Before use, the steel substrates were degreased and prepared as described elsewhere [2,3], in order to assure the realisation of each experiment on a clean and reproducible surface.

Electrodeposition and voltammetry experiments took place in an electrolyte solution containing  $1.30 \text{ M ZnSO}_4 \cdot 7\text{H}_2\text{O}$ ,  $0.18 \text{ M NaCl}$  and  $0.16 \text{ M H}_3\text{BO}_3$ , prepared using analytical grade reagents and deionised water. The pH of the as-prepared bath was approximately 4.6 and was adjusted between 2.0 and 4.5 by addition of dilute sulphuric acid. The temperature was held constant at  $50 \pm 1^\circ\text{C}$ . A rotating disc electrode was employed in order to investigate the effect of cathode rotation on current density. During bulk electrodeposition of Zn, the cathode rotation velocity was kept constant at 800 rpm. Potentiostatic current–time transients (CTTs) were recorded at various cathodic potentials, i.e.  $-1.10$ ,  $-1.15$ ,  $-1.30$ ,  $-1.55$  and  $-2.10 \text{ V}$ , lying within the experimental range of potentials used for the galvanostatic bulk electrodeposition of Zn [3].

The deposits were examined by X-ray diffraction (XRD; Siemens D5000, Cu  $K\alpha$  radiation), while SEM images were taken by a JEOL JSM 6100 apparatus.

### 3. Results and discussion

Voltammetry was first employed in the acidic sulphate solution to identify the potential region for deposition at each bath pH. The potential was scanned towards the cathodic direction, from  $-0.50$  up to  $-2.50 \text{ V}$  vs. SCE. In Fig. 1, the obtained current density–potential curves are shown in a semi-logarithmic scale for three different pH values. In the present system, the pH-independent equilibrium redox potential of the  $\text{Zn}^{2+}/\text{Zn}$  couple was found to be  $-1.01 \text{ V}$ . The observed increase in current at less cathodic potentials, which is particularly intense for pH 2.0–2.5, is due to cathodic hydrogen evolution. For the vertex potential shown ( $-2.50 \text{ V}$ ), a kinetic, Tafel type, current–voltage dependence appears to predominate over the applied potential range indicating that the zinc deposition process is controlled by charge transfer, as was expected on account of the high zinc concentration in the bath. This was verified by measuring the current at various cathode rotation velocities as shown in Fig. 2, where the reciprocal of current density ( $j^{-1}$ ) value appears to be totally independent on cathode rotation velocity ( $\omega^{-1/2}$ ) within the applied working potential range, except near the equilibrium value, where a transport process on the surface may assist the incorporation of zinc atoms to the developing phase.

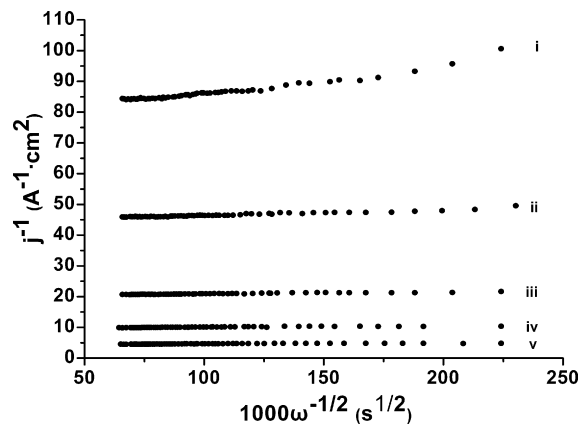


**Fig. 2.** Koutecký-Levich plots ( $j^{-1}$  vs.  $\omega^{-1/2}$ ) with a low-carbon steel rotating disc electrode in the typical sulphate deposition bath (pH 4.0) at  $50^\circ\text{C}$ , for various potentials  $E$  (V vs. SCE):  $-1.10$  (i);  $-1.15$  (ii);  $-1.30$  (iii);  $-1.55$  (iv);  $-2.10$  (v).

The study of nucleation by electrochemical means offers the certain advantage of electrochemical over thermally driven processing techniques, namely the capability of controlling the available free energy via an electric parameter, i.e. the applied potential. The electrochemical nucleation and growth of metals is commonly investigated by recording potentiostatic CTTs at different cathodic potentials. On this basis, several models have been developed to interpret experimental measurements, based on certain assumptions involving the nucleation mode (instantaneous, progressive), the dimensional type of growth (2D, 3D), the geometry of growth centres, and the rate-determining step of the whole process [11,12].

Differently shaped chronoamperometric curves were recorded at various potential and pH values, and compared to theoretically derived results. Fig. 3 shows a family of CTTs recorded at pH 4.0, representative as to their dependence on potential for all the bath-pH values studied. For potentials more negative than  $-1.30 \text{ V}$  (curves iii–v in Fig. 3), the current density initially increases with time until it obtains a steady state value, which is higher the more cathodic is the applied potential. The shape of the CTTs is in accordance with the theoretical model proposed by Armstrong et al. [13], assuming 3D growth of nuclei that have the geometry of right circular cones, limited by the incorporation of metal ad-atoms in the growing crystal lattice. The initial increase in current density is associated with the formation of growth centres, and is confined by the ingestion of free nucleation sites due to growing crystallites as well as by

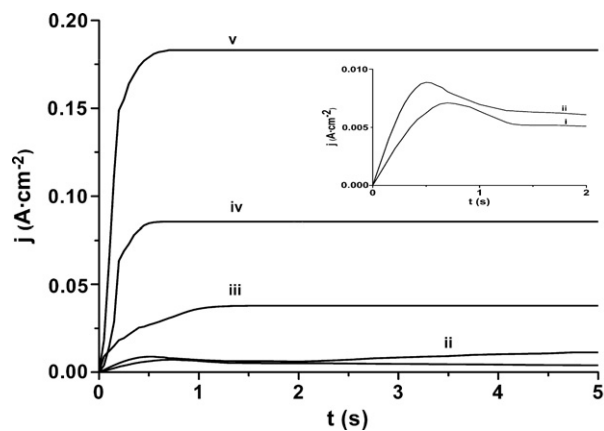


**Fig. 3.** Potentiostatic CTTs on a stationary low-carbon steel electrode in the typical sulphate deposition bath (pH 4.0) at  $50^\circ\text{C}$ , for various potentials  $E$  (V vs. SCE):  $-1.10$  (i);  $-1.15$  (ii);  $-1.30$  (iii);  $-1.55$  (iv);  $-2.10$  (v). The CTTs (i) and (ii) for the low overpotentials, corresponding to  $j < 0.01 \text{ A cm}^{-2}$ , are shown at a larger scale in the inset.

the overlapping of neighbouring crystallites. Each nucleus grows parallel and perpendicular to the substrate surface with different rates, in general, as governed by the atomic density of the developing planes. A general description of the CTTs due to nucleation and growth of right circular cones is given by Eq. (1) [14]:

$$j = nFk' \cdot \left\{ 1 - \exp \left[ -\frac{N_0 \pi k^2 M^2}{\rho^2} \cdot \left( t^2 - \frac{2t}{A} + \frac{2}{A^2} - \frac{2}{A^2} \exp(-At) \right) \right] \right\} \quad (1)$$

where  $j$  ( $\text{A cm}^{-2}$ ) is the current density,  $t$  (s) the time,  $n \cdot F$  ( $\text{C mol}^{-1}$ ) the molar charge transferred during electrodeposition,  $M$  ( $\text{g mol}^{-1}$ ) and  $\rho$  ( $\text{g cm}^{-3}$ ) the molar mass and the density of the deposit,  $k$  and  $k'$  ( $\text{mol cm}^{-2} \text{s}^{-1}$ ) the rate constants for lateral and perpendicular to the substrate surface growth,  $N_0$  ( $\text{cm}^{-2}$ ) the number of preferred nucleation sites per unit area of the substrate, and  $A$  ( $\text{s}^{-1}$ ) the nucleation rate constant, assuming that nucleation follows first order kinetics.

In case of instantaneous nucleation, all nuclei are of similar size and age. The nucleation rate is too high and the number of nuclei is assumed to remain constant during the growth process. The limiting form of Eq. (1) for instantaneous nucleation along with its validity condition reads [14]

$$j = nFk' \cdot \left[ 1 - \exp \left( -\frac{N_0 \pi k^2 M^2}{\rho^2} \cdot t^2 \right) \right] \quad \left( \frac{A}{k\sqrt{N_0}} \geq 60 \frac{M}{\rho} \right) \quad (2)$$

When progressive, the nucleation rate is low and new nuclei are continuously formed during the growth process. The limiting form of Eq. (1) for the progressive type is given by Eq. (3):

$$j = nFk' \cdot \left[ 1 - \exp \left( -\frac{AN_0 \pi k^2 M^2}{3\rho^2} \cdot t^3 \right) \right] \quad \left( \frac{A}{k\sqrt{N_0}} \leq \frac{M}{20\rho} \right) \quad (3)$$

Given that for bulk zinc  $M = 65.37 \text{ g mol}^{-1}$  and  $\rho = 7.14 \text{ g cm}^{-3}$ , the nucleation mode should be purely instantaneous when  $A / (k\sqrt{N_0}) \geq 550 \text{ mol}^{-1} \text{ cm}^{-3}$ , and progressive when  $A / (k\sqrt{N_0}) \leq 0.45 \text{ mol}^{-1} \text{ cm}^{-3}$ .

According to Eqs. (1)–(3), the current density increases with time and tends asymptotically to the value  $nFk'$ , whence the vertical growth rate constant  $k'$  can be calculated. The experimental CTTs were fitted to the above equations by the non-linear regression method using MATLAB software. The square of the correlation coefficient was in all cases greater than 0.95, indicating a good coincidence of the theoretical to the experimental transients (Fig. 4), so that the nucleation type could be specified and the  $A$ ,  $k^2 \cdot N_0$  or

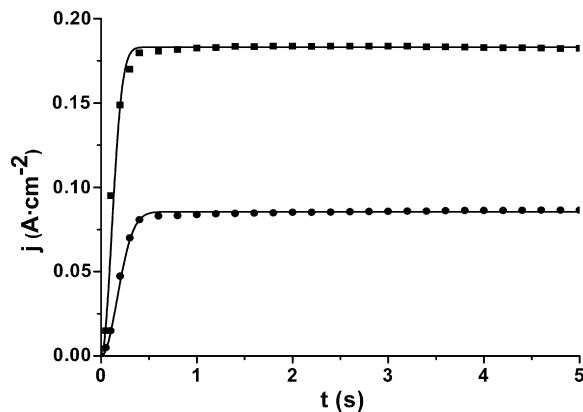


Fig. 4. Fitting of the experimental CTTs presented in Fig. 3 for  $E = -1.55 \text{ V}$  (●) and  $-2.10 \text{ V}$  (■) vs. SCE, to Eq. (2) (—).

$k^2 \cdot A \cdot N_0$  terms could be estimated from Eqs. (1)–(3). The kinetic parameters, calculated by the fitting procedure, are presented in Tables 1 and 2. It is observed that, in general, both  $k'$  and  $k^2 \cdot N_0$  values are potential-dependent and increase with cathodic potential.

The analysis of the results showed that for cathodic overpotentials higher than 0.30 V, instantaneous nucleation was predominant in the major part of the experimental conditions, while for overpotentials higher than 0.55 V and very acidic baths, progressive nucleation prevailed. The change of instantaneous to progressive nucleation can be clearly associated to the strong adsorption of  $\text{H}^+$  species on the cathode at highly cathodic potentials and/or low-pH solutions, which results in inhibition of the metal deposition process, as blocking active sites for  $\text{Zn}^{2+}$  discharge [15].

Let us consider now the CTTs obtained at potentials less negative than  $-1.30 \text{ V}$ , i.e. at overpotentials lower than 0.30 V. In Fig. 3, the respective curves i and ii, scaled-up in the inset, are seen to reach a maximum at short time and then decay at a decreasing rate, so that the deposition current tends to obtain a stationary value. Both the maximum and the steady-state value increase with potential. The shape of the experimental transients implies that the very initial stage of the new phase formation may be appropriately illustrated by a 2D nucleation/growth model. Thus, following the description of Bewick et al. [16], the deposition process is considered to be controlled by the rate of incorporation of Zn ad-atoms at the periphery of expanding growth centres having the shape of cylindrical discs, one atom thick from base to base, which coalesce to form one monolayer after the other. Then, the observed maximum of the current is associated to the completion of the first layer of the new phase, and the nucleation mode for this layer can be identified by considering the variation of  $(j/j_m)$  vs.  $(t/t_m)$ , as given by Eqs. (4) and (5) for instantaneous and progressive nucleation, respectively [17],  $t_m$  being the time corresponding to the maximum observed current

Table 1  
Kinetic parameters obtained by fitting Eq. (2) to the experimental CTTs.

E (V vs. SCE)	pH 2.0		pH 2.5		pH 3.0	
	$k'$ ( $\times 10^7 \text{ mol cm}^{-2} \text{ s}^{-1}$ )	$k^2 \cdot N_0$ ( $\text{mol}^2 \text{ cm}^{-6} \text{ s}^{-2}$ )	$k'$ ( $\times 10^7 \text{ mol cm}^{-2} \text{ s}^{-1}$ )	$k^2 \cdot N_0$ ( $\text{mol}^2 \text{ cm}^{-6} \text{ s}^{-2}$ )	$k'$ ( $\times 10^7 \text{ mol cm}^{-2} \text{ s}^{-1}$ )	$k^2 \cdot N_0$ ( $\text{mol}^2 \text{ cm}^{-6} \text{ s}^{-2}$ )
-1.30		$N_0$ fit	$2.20 \pm 0.04$	$0.0316 \pm 0.0056$	$2.08 \pm 0.03$	$0.0340 \pm 0.0059$
-1.55	$4.69 \pm 0.02$	$0.2657 \pm 0.0246$	$4.30 \pm 0.02$	$0.1594 \pm 0.0108$	$4.26 \pm 0.04$	$0.0153 \pm 0.0012$
-2.10	Progressive nucleation		Progressive nucleation		$8.73 \pm 0.13$	$0.0517 \pm 0.0091$
E (V vs. SCE)	pH 3.5		pH 4.0		pH 4.5	
	$k'$ ( $\times 10^7 \text{ mol cm}^{-2} \text{ s}^{-1}$ )	$k^2 \cdot N_0$ ( $\text{mol}^2 \text{ cm}^{-6} \text{ s}^{-2}$ )	$k'$ ( $\times 10^7 \text{ mol cm}^{-2} \text{ s}^{-1}$ )	$k^2 \cdot N_0$ ( $\text{mol}^2 \text{ cm}^{-6} \text{ s}^{-2}$ )	$k'$ ( $\times 10^7 \text{ mol cm}^{-2} \text{ s}^{-1}$ )	$k^2 \cdot N_0$ ( $\text{mol}^2 \text{ cm}^{-6} \text{ s}^{-2}$ )
-1.30	$1.89 \pm 0.06$	$0.0258 \pm 0.0091$	$1.96 \pm 0.05$	$0.0117 \pm 0.0027$	$1.77 \pm 0.04$	$0.0084 \pm 0.0015$
-1.55	$4.74 \pm 0.07$	$0.0379 \pm 0.0058$	$4.43 \pm 0.02$	$0.0687 \pm 0.0047$	$3.67 \pm 0.05$	$0.0263 \pm 0.0036$
-2.10	$9.06 \pm 0.02$	$0.2446 \pm 0.0124$	$9.48 \pm 0.02$	$0.1593 \pm 0.0055$	$9.57 \pm 0.03$	$0.1815 \pm 0.0093$

**Table 2**  
Kinetic parameters obtained by fitting Eq. (3) to the experimental CTTs.

E (V vs. SCE)	pH 2.0		pH 2.5	
	$k' (\times 10^7 \text{ mol cm}^{-2} \text{ s}^{-1})$	$k^2 \cdot A \cdot N_0 (\text{mol}^2 \text{ cm}^{-6} \text{ s}^{-3})$	$k' (\times 10^7 \text{ mol cm}^{-2} \text{ s}^{-1})$	$k^2 \cdot A \cdot N_0 (\text{mol}^2 \text{ cm}^{-6} \text{ s}^{-3})$
-2.10	$9.28 \pm 0.06$	$0.5081 \pm 0.0532$	$9.06 \pm 0.07$	$0.2557 \pm 0.0258$

density  $j_m$ :

$$\frac{j}{j_m} = \frac{t}{t_m} \exp \left[ -\frac{(t^2 - t_m^2)}{2t_m^2} \right] \quad (4)$$

$$\frac{j}{j_m} = \frac{t^2}{t_m^2} \exp \left[ -\frac{2(t^3 - t_m^3)}{3t_m^3} \right] \quad (5)$$

In Fig. 5, the experimental measurements are plotted in common axis with the theoretical curves, within the initial peak width wherein the relations (4) and (5) are valid. A fairly good agreement is observed, suggesting progressive 2D nucleation for pH 2.5, and instantaneous 2D nucleation for pH 4.0. Certainly, the theoretical currents vanish after formation of a single layer, since the exponential terms decrease faster than their coefficients increase with time, whereas the experimental current obtains a steady-state value. This might be correlated to the prediction of the above model in its more elaborated form; the formation of successive layers under conditions of 2D nucleation and growth by incorporation of Zn ad-atoms at the expanding growth centres, either involving surface diffusion or not, is actually a manageable theoretical problem [18]. However a realistic description of the present results, concerning metal deposition on an imperfect substrate inhibiting the spreading of single layers, is not susceptible to an accurate analysis. Then, the average current density generated from developing multiple grains and succeeding layers will be reasonably attributed to a degenerating 2D nucleation/growth process, being significant at the relatively strain-free domains of the deposition substrate, involving a 3D growth character as well.

Our previous results on zinc electrodeposition from similar solutions on steel [3] have shown that bulk deposits exhibiting various well-defined crystallographic textures are produced in the major part of the experimental conditions (Fig. 6). Specifically, high current densities ( $> \text{ca. } 0.05 \text{ A cm}^{-2}$ ) and very acidic baths ( $\text{pH} < 3.0$ ) promote intense basal (00.2) texture (Fig. 7), whereas for low “supersaturation”, i.e. current densities lower than about  $0.01 \text{ A cm}^{-2}$ , randomly oriented layers are obtained (Fig. 8).

The texture of a deposit with thickness in the  $\mu\text{m}$  order is determined mainly by the electrolysis conditions and not the substrate, whose effect rapidly attenuates [19]; however, the electrolysis

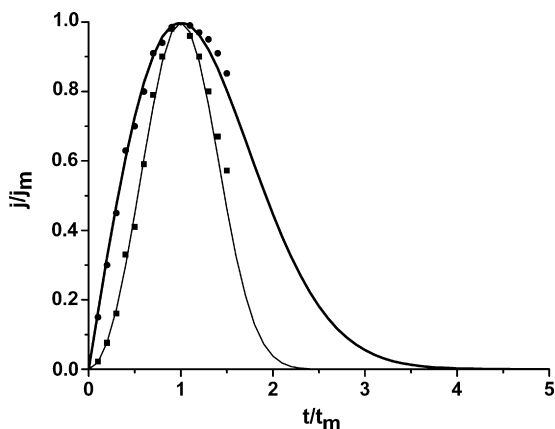


**Fig. 5.** Dimensionless curves ( $j/j_m$ ) vs. ( $t/t_m$ ) for instantaneous (thick line) and progressive (thin line) 2D nucleation from Eqs. (4) and (5) respectively, along with experimental points for pH 2.5 (■) and pH 4.0 (●), at  $-1.10 \text{ V vs. SCE}$ .

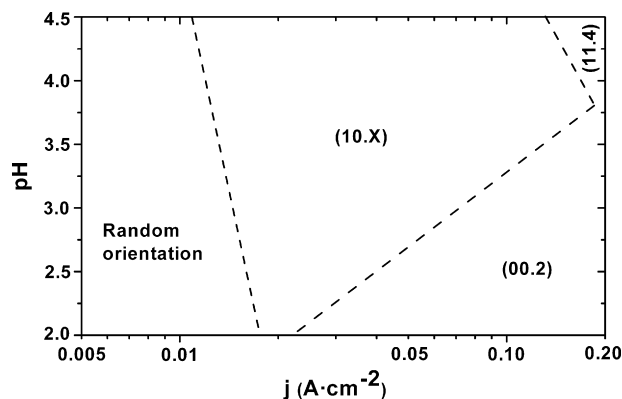


**Fig. 6.** Simplified diagram of crystallographic textures as a function of deposition current density and bath pH, for zinc electrodeposits obtained from acidic sulphate bath on low-carbon steel, under DC conditions. The texture designation was derived according to the Relative Texture Coefficient (RTC) statistical method [1,3].

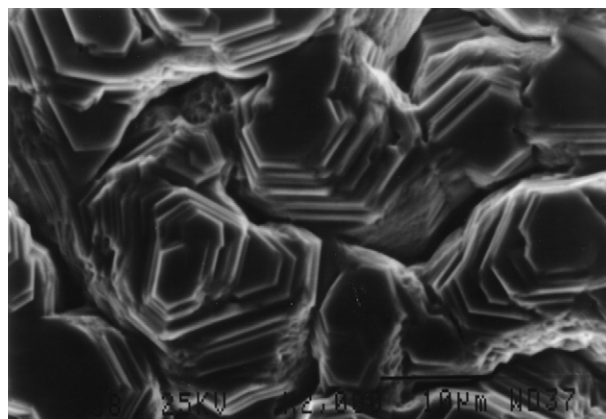


**Fig. 7.** SEM micrograph of a zinc electrodeposit obtained from a pH 2.0 bath, under DC conditions, at  $j = 0.20 \text{ A cm}^{-2}$ . The coating consists of a basal stacking sequence of well-formed hexagonal crystals, exhibiting a clear (00.2) crystallographic texture.

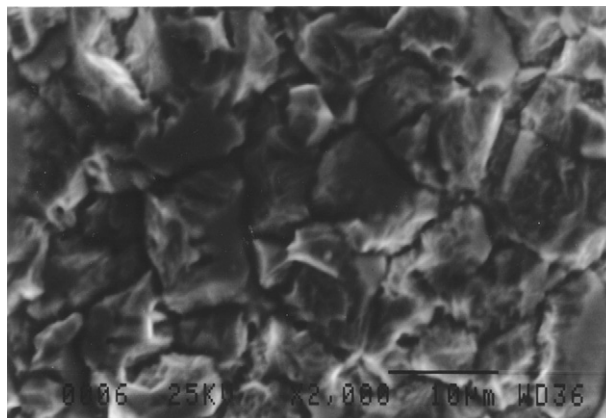


**Fig. 8.** SEM micrograph of a randomly oriented zinc electrodeposit obtained from a pH 2.0 bath, under DC conditions, at  $j = 0.005 \text{ A cm}^{-2}$ .

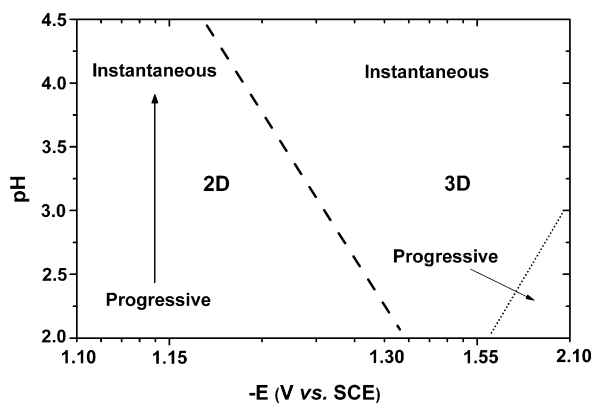


Fig. 9. Simplified diagram of dominant nucleation and growth modes in the range of conditions used to electrodeposit zinc from typical sulphate bath on low-carbon steel, under DC conditions. The cathodic potentials correspond to the respective current densities of the texture diagram (Fig. 6).

parameters determine also the type of nucleation. Hence it would be useful to establish a correlation involving the type of charge-transfer controlled nucleation on the steel electrode and the XRD texture of the final deposit. Fig. 9 shows the nucleation and growth modes as estimated from the present analysis of experimental CTTs for various conditions. By inspection of the corresponding texture domains in Fig. 6 one can see that a well-defined texture, i.e. oriented growth, is connected to 3D nucleation, while the absence of a plain orientation is connected to the assumed mixed dimensionality mechanism. The latter occurs for deposition potentials near the equilibrium value which actually promote a 2D layer-by-layer growth, restrained though for the most part as a result of the non-uniform distribution of active nucleation sites and defects on the steel substrate. Under these circumstances, the initially disturbed growth leads to the formation of slightly misoriented crystallites which give rise finally to a deposit without any dominant texture, because the low-supersaturation conditions are not capable of restoring a directional growth.

Finally, as an illustration of the complexities involved in determining reasonable parameters of the nucleation process, the classical theory of heterogeneous nucleation will be used to estimate analytically the critical size of the three-dimensional nuclei assumed to initiate the construction of the deposit grains for overpotentials greater than 0.30 V. In this theory, the radius  $r_{\text{crit}}$  (cm) of the circular base of a critical nucleus is given by Eq. (6) [20]:

$$r_{\text{crit}} = \frac{2M\sigma}{\rho nF|\eta|} \quad (6)$$

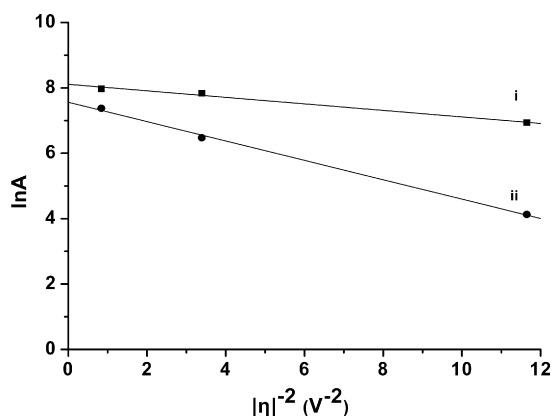


Fig. 10. Plot of  $\ln A$  vs.  $|\eta|^{-2}$  according to data obtained from the non-linear regression analysis of the experimental CTTs recorded at pH 2.5 (i) and pH 4.0 (ii).

where  $|\eta|$  (V) is the overpotential,  $\sigma$  ( $\text{J cm}^{-2}$ ) the interfacial energy, and the other symbols as described previously.

The nucleation rate constant presents an exponential dependence on  $(1/|\eta|)^2$  according to Eq. (7):

$$\ln A = \ln B_j - \frac{8\pi M^2 \sigma^3}{3\rho^2 n^2 F^2 k_B T} \cdot \frac{1}{|\eta|^2} \quad (7)$$

where  $B_j$  ( $\text{s}^{-1}$ ) is a frequency factor,  $k_B$  the Boltzmann constant, and  $T$  (K) is the temperature. Therefore, the interfacial energy could be calculated from the slope of  $\ln A$  vs.  $|\eta|^{-2}$  plots using the values estimated for the nucleation rate constant  $A$ . The slopes were found to be  $-0.11$  and  $-0.35 \text{ V}^2$  for pH 2.5 and 4.0, respectively (Fig. 10), giving an interfacial energy for Zn nuclei in the range  $2.96 \times 10^{-5}$ – $4.37 \times 10^{-5} \text{ J cm}^{-2}$ . Substituting these values to Eq. (6), the radius of the circular base of the critical nucleus was found to lie between 26 and 142 pm. However, the atomic radius of a Zn atom is known to be 133 pm, while the classical theory is strictly valid when the nucleus contains an appreciable number of atoms (at least a hundred) [21]. Consequently, the estimated radius of the critical nucleus is too small to be consistent with this simple theory. More sophisticated approaches, e.g. those based on the atomistic theory of nucleation [21,22], should have a more realistic outcome.

#### 4. Conclusions

A systematic study of zinc electrocrystallisation on low-carbon steel from an acidic sulphate medium, under charge transfer control, was performed. Depending on applied potential and bath pH, different nucleation and growth modes were identified.

At cathodic overpotentials less than 0.30 V, a 2D-nucleated layer-by-layer growth strained by the substrate effect is established, rapidly degenerating to a 3D type of growth. At overpotentials higher than 0.30 V, instantaneous 3D nucleation and growth was found to be predominant, while progressive 3D nucleation was seen to prevail at overpotentials greater than 0.55 V and highly acidic baths. Progressive nucleation was generally dominant at low pH values, as the intense hydrogen adsorption in these conditions, inhibits the active nucleation sites. The electrocrystallisation process was controlled by the incorporation of Zn ad-atoms in the solid lattice.

The radius of the critical nucleus for zinc nucleation, as estimated by means of the classical theory of heterogeneous nucleation, was found to be in the range 26–142 pm corresponding to maximum one zinc atom. Since the classical theory is strictly valid when the nucleus contains an appreciable number of atoms, alternative approaches should be employed in order to get satisfactory results in this connection.

#### References

- [1] X. Ye, J.P. Celis, M. De Bonte, J.R. Roos, J. Electrochem. Soc. 141 (1994) 2698.
- [2] D. Vasilakopoulos, M. Bouroushian, N. Spyrellis, J. Mater. Sci. 41 (2006) 2869.
- [3] D. Vasilakopoulos, M. Bouroushian, N. Spyrellis, Trans. IMF 79 (2001) 107.
- [4] K. Raeissi, A. Saatchi, M.A. Golozar, J. Appl. Electrochem. 33 (2003) 635.
- [5] K. Raeissi, A. Saatchi, M.A. Golozar, J.A. Szpunar, J. Appl. Electrochem. 34 (2004) 1249.
- [6] A. Gomes, M.I. da Silva Pereira, Electrochim. Acta 51 (2006) 1342.
- [7] V. Velinov, E. Beltowska-Lehman, A. Riesenkamp, Surf. Coat. Technol. 29 (1986) 77.
- [8] A.E. Alvarez, D.R. Salinas, J. Electroanal. Chem. 566 (2004) 393.
- [9] J. Torrent-Burgués, E. Gaus, J. Appl. Electrochem. 37 (2007) 643.
- [10] A. Gomes, A.S. Viana, M.I. da Silva Pereira, J. Electrochem. Soc. 154 (2007) D452.
- [11] P.J. Sonneveld, W. Visscher, E. Barendrecht, Electrochim. Acta 37 (1992) 1199.
- [12] R. Greef, R. Peat, L.M. Peter, D. Pletcher, J. Robinson, Instrumental Methods in Electrochemistry, Ellis Horwood, London, 1993 (Chapter 9).
- [13] R.D. Armstrong, M. Fleischmann, H.R. Thirsk, J. Electroanal. Chem. 11 (1966) 208.

- [14] M.Y. Abyaneh, J. Electroanal. Chem. 530 (2002) 82.
- [15] C. Cachet, R. Wiart, J. Electrochem. Soc. 141 (1994) 131.
- [16] A. Bewick, M. Fleischmann, H.R. Thirsk, Trans. Faraday Soc. 58 (1962) 2200.
- [17] J.A. Harrison, H.R. Thirsk, Electroanal. Chem. 5 (1971) 67.
- [18] R.D. Armstrong, J.A. Harrison, J. Electrochem. Soc. 116 (1969) 328.
- [19] J. Amblard, M. Froment, G. Maurin, D. Mercier, E. Trevisan-Pikacz, J. Electroanal. Chem. 134 (1982) 345.
- [20] M.Y. Abyaneh, M. Fleischmann, J. Electroanal. Chem. 530 (2002) 89.
- [21] A. Milchev, S. Stoyanov, R. Kaishev, Thin Solid Films 22 (1974) 255.
- [22] E. Budevski, G. Staikov, W.J. Lorenz, Electrochim. Acta 45 (2000) 2559.